World Academy of Science, Engineering and Technology
International Journal of Geotechnical and Geological Engineering
Vol:18, No:9, 2024

Influence of Loading Pattern and Shaft Rigidity on Laterally Loaded Helical Piles in Cohesionless Soil

Mohamed Hesham Hamdy Abdelmohsen, Ahmed Shawky Abdul Aziz, Mona Fawzy Al-Daghma

Abstract**—**Helical piles are widely used as axially and laterally loaded deep foundations. When they are required to resist bearing combined loads (BCLs), such as axial compression and lateral thrust, different behaviour is expected, necessitating further investigation. The aim of the present article is to clarify the behaviour of a single helical pile of different shaft rigidity embedded in cohesionless soil and subjected to simultaneous or successive loading patterns of BCLs. The study was first developed analytically and extended numerically. The numerical analysis using PLAXIS 3D was further verified through a laboratory experimental programme on a set of helical pile models. The results indicate highly interactive effects of the studied parameters, but it is obviously confirmed that the pile performance increases with both the increase of shaft rigidity and the change of BCLs loading pattern from simultaneous to successive. However, it is noted that the increase of vertical load does not always enhance the lateral capacity but may cause a decrement in lateral capacity, as observed with helical piles of flexible shafts. This study provides insightful information for the design of helical piles in structures loaded by complex sequence of forces, wind turbines, and industrial shafts.

Keywords**—**Helical pile, lateral loads. combined loads, cohesionless soil, analytical model, PLAXIS 3D.

I. Introduction

HELICAL piles are ready-made steel piles. Practice observations proved these piles possess advantages over conventional straight piles under the action of both tension and compression axial loads [1], [2]. Recently, emphasis has been raised on the ability of helical piles to withstand the effects of lateral loads, especially for wind turbines, solar panels, and offshore structures [1], [3]-[8]. Field tests [9]-[12] confirmed that helical piles can develop significant lateral resistance. Laboratory experimental studies [13]-[16] were also conducted to investigate the lateral resistance of multi-helix piles in sandy soils. The studies concluded that the lateral capacity increased with the increase in helix number and that the most efficient spacing between helices is approximately three times the diameter of the pile shaft. Furthermore, the best locations of the helices are observed within 1/3 to 1/2 the pile length. As well, many researchers have investigated the behaviour of helical piles under vertical or lateral loading using numerical analysis and the same behaviour was realised [17]-[23]. Analytically, Mittal et al. [13] developed a theoretical model to calculate the lateral capacity of helical piles, however, rigidity conditions and loading criteria were not considered.

Previous studies investigated deeply the behaviour of helical piles against either axial or lateral loading. However, there is a lack of studies that considered combinations of vertical and horizontal loads, "Combined loads". Understanding the behaviour of helical piles under this loading condition is essential for supporting structures such as renewable energy structures, which require substantial expenditures. Few researchers have addressed this case of loading. Numerical studies simulating helical piles under combined loading in sand were conducted using PLAXIS 3D by Al-Baghdadi et al. [17]. This study indicated that the increase in axial compression loads enhances lateral capacity, and the opposite effect is observed with axial tension load. In addition, two models of piles were studied, assumed short and long. The short pile showed better lateral improvement under the combined loading effect in comparison to the long one.

Also, combined loading was studied using ABAQUS 2018 by [1], [18]. Pavan Kumar et al. [1] concluded that the point of maximum lateral stress is the best location of the helix at which the lateral capacity is increased by approximately 16% for single or multi-helix pile models, but regrettably, this location was geometrically undefined. Pavan Kumar et al. [18] validated that the helical pile may be a viable alternative to conventional concrete piles for wind turbine foundations because of its high capacity, and well behaviour under combined load which can be optimised for maximum lateral load. Moreover, the study found that the capacity of double-helical piles exceeds single-helical piles under combined load conditions by 59%.

In view of the above, research concentrated on helical piles loaded vertically or laterally. Moreover, there is a lake of studies considering a combination of vertical and horizontal loading, which more accurately reflects the real loading conditions. Also, the variation of shaft rigidity has not ever been investigated which causes a considerable effect on the lateral capacity of helical piles. Consequently, this study is a pioneer in consideration of different parameters; shaft rigidity, pile geometry, optimal helix location and combined loading modes either simultaneous or successive. The current paper studies the behaviour of a single vertical helical pile embedded in cohesionless soil under BCLs using firstly an analytical simplified model. Later, a FEM using PLAXIS 3D which

H. H. Abdelmohsen is Professor with Dept. of Structural Engineering, Alexandria University, Postal Code 21544, Egypt (e-mail: mohamed.abdelmohsen@alexu.edu.eg).

Ahmed Shawky Abdul Aziz is Associate Professor with Dept. of Structural Engineering, Alexandria University, Postal Code 21544, Egypt (e-mail: abdulazizahmed646@alexu.edu.eg).

Mona F. Aldaghma is Ph.D. Student with Dept. of Structural Engineering, Alexandria University, Postal Code 21544, Egypt and Assistant Lecturer with Department of Construction and Engineering Management, Pharos University, Postal Code 21311, Egypt (corresponding author, ORCID: https://orcid.org/0000-0002-5381-2227, e-mail: mona.fawzy@alexu.edu.eg).

verified by a laboratory experimental program and field loading test by Elsherbiny et al. [22].

II. Analytical Model

A. Model Assumptions

The analytical model assumes the following:

1. The soil is homogeneous, isotropic and cohesionless with constant stiffness parameters [24].
2. The rigidity conditions of the straight pile and of the helical pile shaft are the same.
3. The pile shaft–soil interface is frictionless.
4. The ultimate lateral displacement of the pile shaft is at the ground surface with a value equal to 10% of the helix diameter.
5. For simplicity, the helix is treated as a rigid solid square plate of width D and bearing capacity equations for deep or shallow foundations [25] are applicable according to the helix location below the ground surface.
6. The combined loads, Q and V, act in two loading modes, simultaneous and successive. To differentiate between the two modes, it is assumed that under simultaneous loading, soil properties, such as unit weight (γ) and angle of internal friction (φ), are constant during loading, whereas, under successive loading, the soil below the helix is compacted by the vertical preload (V) and a volumetric change occurs causing a decrease in the void ratio (e) and thus an increase in both (γ) and (φ) are increased.
7. The lateral resistance of a helical pile (Q) is the sum of three components, Fig. 1: horizontal friction between the helix plate and the soil below it (Q_F), bearing resistance between the helix plate and the soil (Q_M), and the lateral resistance of the pile shaft (Q_o), which corresponds the resistance of a straight pile without helix.
8. The lateral resistance (Q) is initially started as Q_F and gradually increases due to the combined resistance ($Q^* = Q_o + Q_M$). Accordingly, lateral resistance is represented as:

$$Q = Q_F + Q^* \tag{1}$$

B. Model Development

The initial friction resistance, Q_F can be estimated as:

$$Q_F = V \tan(\varphi^*) \left(\frac{L-H}{L}\right) \tag{2}$$

where V is the acting vertical load on the pile head, φ^* is the angle of friction between the helix plate and soil, L is the pile length embedded into the soil, and H is the depth below ground surface at which the helix plate exists.

The lateral resistance of a straight pile (i.e., the pile shaft resistance (Q_o) is related to the lateral displacement (δx_o) at ground surface, [26], as:

$$\delta x_o = Q_o \left(\frac{I_1}{E_s L_e} + \frac{Y I_2}{E_s L_e^2}\right) \tag{3}$$

where E_s is the soil elastic modulus, L_e is the effective pile length, Y is the free length of the pile shaft above ground surface, I_1 and I_2 are influencing factors depending on the pile's relative rigidity (i.e., the pile is either rigid, flexible, or intermediate), which is related to the critical length (L_c) [26] as:

$$L_c = 4.44 \sqrt[4]{\frac{E_p I_p}{E_s}} \tag{4}$$

E_p is the elastic modulus of pile material, I_p is the moment of inertia of the pile shaft cross-section. Referring to (1), where L is the length of the pile inserted into the ground, for $L > L_c$, the pile is a flexible (long) pile; for $L < \frac{L_c}{3}$, the pile is a rigid (short); and for $\frac{L_c}{3} \leq L \leq L_c$, the pile is intermediate [26]. For flexible piles, $L_e = L_c$; for rigid piles, $L_e = L$; and for intermediate piles, L_e could be considered as the average of the two cases, rigid and flexible.

At the limit equilibrium of the pile under the action of the two components of the combined load, Q and V, the maximum value of the bearing stress q_b should be the ultimate bearing capacity of the soil at the level of the helical plate (Fig. 2) and the following set of equations are generated:

$$f_V = \frac{V}{A_h} \tag{5}$$

$$f_m = q_b - f_V \tag{6}$$

$$\text{At } \left(\frac{H}{D} < 5.00\right) \ldots\ldots q_b = \gamma_1 H N_q S_q + \frac{1}{2} \gamma_2 D N_\gamma S_\gamma \tag{6a}$$

$$\text{At } \left(\frac{H}{D} \geq 5.00\right) \ldots\ldots q_b = \gamma_1 H N_q^* \tag{6b}$$

$$M_h = \frac{1}{6} f_m (D^3) \tag{7}$$

where (6a) and (6b) are the ultimate bearing capacity of shallow and deep foundations [27] and will be applied for shallow or deep helical plates [25]. N_q, $N_q^* and\ N_\gamma$ are bearing capacity factors, $S_q$and S_γ are shape factors, γ_1 and γ_2 are the unit weights of soil above and below the helix plate, respectively and A_h is the bearing area of the helix plate. The effect of the equivalent resisting moment, (M_h), could be considered either as a reverse lateral displacement, (δx^*) for flexible pile, or as a reverse lateral load, (ΔQ), for rigid pile, [28] where:

$$\delta x^* = \frac{B_x M_h T^2}{E_p I_p} \tag{8}$$

$$T = \sqrt[5]{\frac{E_p I_p}{n}} \tag{9}$$

$$\Delta Q = \frac{M_h}{H} \tag{10}$$

where B_x is an influence factor for estimating the distribution of lateral displacements along the pile shaft according to the location of the acting moment [29], n is the coefficient of

horizontal subgrade reaction of soil around the pile shaft and H is the depth at which the helix is located below the ground surface, Fig. 1.

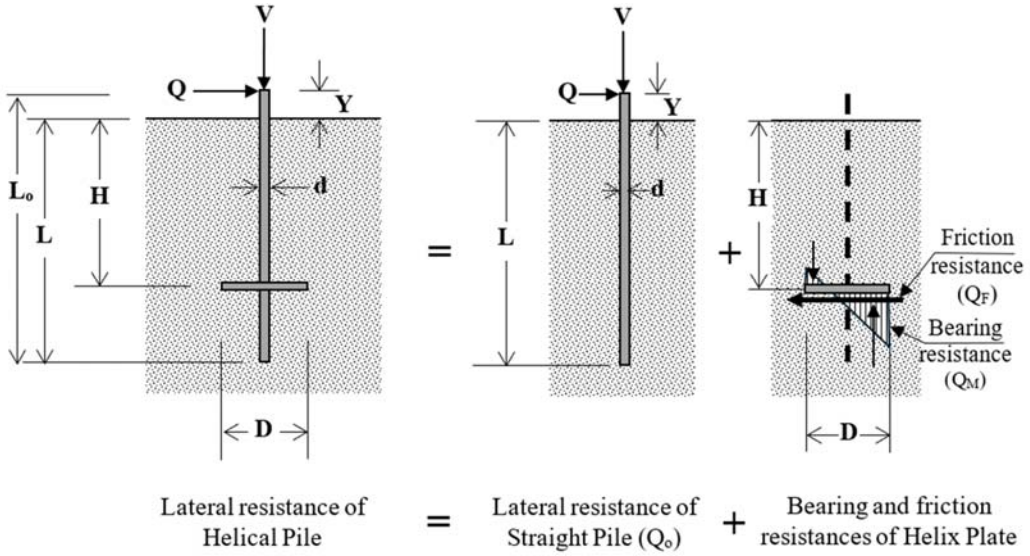

Fig. 1 Diagrammatic representation of the analytical model

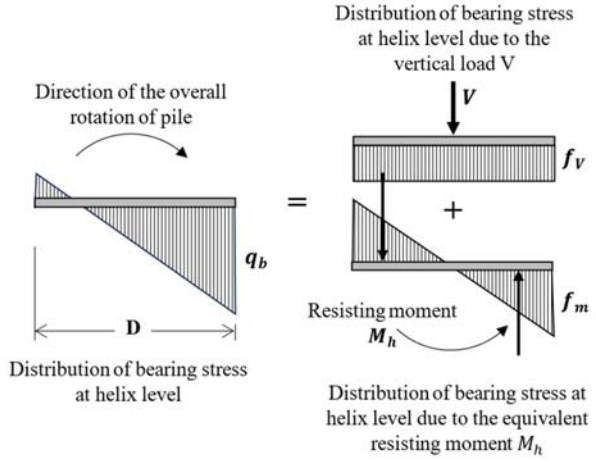

Fig. 2 Bearing stresses at the helix level

Considering that the limit of the net lateral displacement of the helical pile at ground surface (δx_{net} = 10% D), then:

- For flexible helical piles, the corresponding lateral resistance (Q^*) can be estimated from:

$$\delta x_{net} = \delta x_o - \delta x^* = 0.10\,(D)\,.. \tag{11}$$

Substituting (3) and (8) into (11),

$$Q^*\left(\frac{I_1}{E_s\,L_e} + \frac{Y\,I_2}{E_s\,L_e^2}\right) = 0.10\,D + \left(\frac{B_x\,T^2}{E_p\,I_p}\right)M_h \tag{12}$$

- For rigid helical piles, the lateral resistance Q^* can be estimated as:

$$Q^* = Q_o + \Delta Q \tag{13}$$

where Q_o and ΔQ are obtained from (3) and (10) respectively, considering that $\delta x_{net} = 10\%\,D$.

$$Q^* = 0.10\,\frac{D}{\left(\frac{I_1}{E_s\,L_e} + \frac{Y\,I_2}{E_s\,L_e^2}\right)} + \frac{M_h}{H}\ldots \tag{14}$$

- For intermediate helical piles, the lateral resistance Q^* could be considered as an average value between flexible piles (12) and rigid piles (14) [14].

The lateral resistance of a helical pile is a combined effect due to the presence of the helix and vertical load (V). The improvement ratio (IR) is defined as:

$$IR = \frac{Lateral\ resistance\ of\ helical\ pile\ (Q)\ at\ (V \geq 0)}{Lateral\ resistance\ of\ straight\ pile\ (Q_o)\ at\ (V = 0)}$$

C. Model Applications

Pile models, as manufactured for field practice, are selected to represent the three states of pile shaft rigidity: rigid, flexible, and intermediate. For each state of rigidity, two geometrical categories were considered, A and B, where B-category of dimensions larger than those of category (A). Each model has one helix of diameter (D) located at different depths (H) along the pile length (L). The pile material is steel, with elastic modulus (E_p = 200 × 10^3 MPa). Pile shafts are hollow tubes with outer diameter (d) and wall thickness (t). All pile models are subjected to two modes of BCLs, simultaneous and successive. The surrounding soil is considered as dry sand of medium density with the following properties:

- Initial dry unit weight (γ_o) = 16.00 kN/m^3
- Specific gravity (G_s) = 2.65
- Initial angle of internal friction (φ) = 33°
- Elastic modulus (E_s) = (25 – 40) MPa, [30]
- Poisson's ratio (μ) = 0.30, [30]
- Average coefficient of lateral subgrade reaction (n) = (4000

– 6000) kN/m^3 [30].

As mentioned in Table I, each pile model is presented by a three-symbol Model ID. The first symbol represents the shaft rigidity condition (R, F, or I), the second symbol represents the category of pile geometry (A or B) and the third symbol represents the helix diameter ratio (D/d). Two different helix diameter ratios (D/d) were considered for each pile model, 2.5 and 5.0. The helix depth (H) to the pile length (L) ratio is varied as H/L = 0.1, 0.2, 0.4, 0.6, 0.8 and 0.9. The pile models were subjected to two vertical loads, V1 = Vu/2 and V2 = Vu, where Vu is a constant value for each model, assumed as the ultimate vertical bearing load of a shallow helix plate rested at H/L = 0.10.

TABLE I
PILE MODEL DETAILS

Shaft Rigidity		Model ID	* Geometry D cm	L_o cm	L cm	d cm	t cm	** Rigidity conditions
Rigid **(R)**	A	R-A-2.5 R-A-5.0	81 162	240	200	32.4	9.0	$L < L_c/3$ $L/T < 2$
	B	R-B-2.5 R-B-5.0	101.5 203	300	250	40.6	9.5	
Flexible **(F)**	A	F-A-2.5 F-A-5.0	22 44	450	375	8.8	0.9	$L > L_c$ $L/T > 4$
	B	F-B-2.5 F-B-5.0	81 162	1000	850	32.4	0.9	
Intermediate **(I)**	A	I-A-2.5 I-A-5.0	22 44	180	150	8.8	0.9	$L_c/3 < L < L_c$ $2 < L/T < 4$
	B	I-B-2.5 I-B-5.0	81 162	400	325	32.4	0.9	

* Referring to Fig. 1
** Referring to (4) and (9)

Results and Discussions of Model Applications

The results are presented in two groups. The first group presents the results for pile models subjected to lateral horizontal loads only (V = 0), whereas the second group presents results for the same pile models when subjected to BCLs in the two modes; simultaneous and successive. All the results are best fitted as second- or third-degree polynomial curves.

1. Lateral Horizontal Load (V = 0):

For Fig. 3, the following conclusions are drawn:

- The resistances of rigid and intermediate helical piles against horizontal loads are generally greater than those of the corresponding straight piles, (i.e., IR > 1.00). For flexible helical piles, the same was observed with helices at H/L < 0.40, however for H/L ≥ 0.40, the helices are practically ineffective where the values of IR became almost 1.00 or slightly less (i.e., Fig. 3 (a) explaining the effect of rigidity of category "A"). Mathematically, these findings could be explained as follows:
  - Referring to (3), the numerical values of the factors (I_1) and (I_2) for rigid shafts are much less than those for flexible shafts, then the lateral resistance (Q_o) of rigid shaft is larger than that of flexible shaft. By adding the effect of helices, as δx^* for flexible piles (8), and as ΔQ for rigid piles (10), which are functions of the resisting moment (M_h), the resulting additional resistances for rigid piles are found to be larger than that for flexible piles, which means that the total lateral resistances of rigid helical piles are larger than those of flexible helical piles and of course helical piles of intermediate rigidity should be of intermediate lateral resistances.
  - Also, for flexible piles with helices at H/L ≥ 0.40, according to the corresponding numerical values of the factor B_x, the values of δx^* became almost zero or slightly less, then referring to (12), the lateral resistance of flexible helical piles could be equal to or slightly less than the resistance of flexible straight piles.
- Increasing the piles geometry from category A to category B and increasing the helix diameter ratio (D/d) from 2.50 to 5.00, leading to considerable increasing in IR. These effects become more tangible with the increase of pile shaft rigidity. Mathematical wise, this is a direct result from (1), (2), and (12), for V = 0 (i.e., for rigid model, Fig. 3 (b)).
- For rigid and intermediate helical piles, with helices at H/L ≥ 0.60, the improvement ratio IR is almost constant, i.e., not affected by the variation in helix location. This observation could be attributed to the mostly constant values of δx^* and ΔQ, (8) and (10), respectively. At these deep locations, q_b is mostly calculated from (6b), and M_h from (7), both are increased linearly with H, whereas the factor B_x is decreased with H, then both ΔQ and δx^* become almost constant.

2. Bearing Combined Loads

Using Fig. 4, the findings are as follows:

- The change of loading mode from simultaneous to successive has an insignificant effect on the ratio (IR), except for rigid piles in geometrical category (B) (i.e., Fig. 4 (a)).
  - Referring to Section II *A*– item 6, on the principle of soil densification under successive loading modes, for soil in medium density and the corresponding range of its elastic modulus (E_s), the resulting volumetric changes were very limited causing almost no difference in soil properties, γ and φ. For rigid piles in geometrical category (B), where

the dimensions were significantly large, the densified zone below the helices is large enough to cause considerable volumetric change under the action of successive loading mode which in turn caused the observed increase in (IR) values.

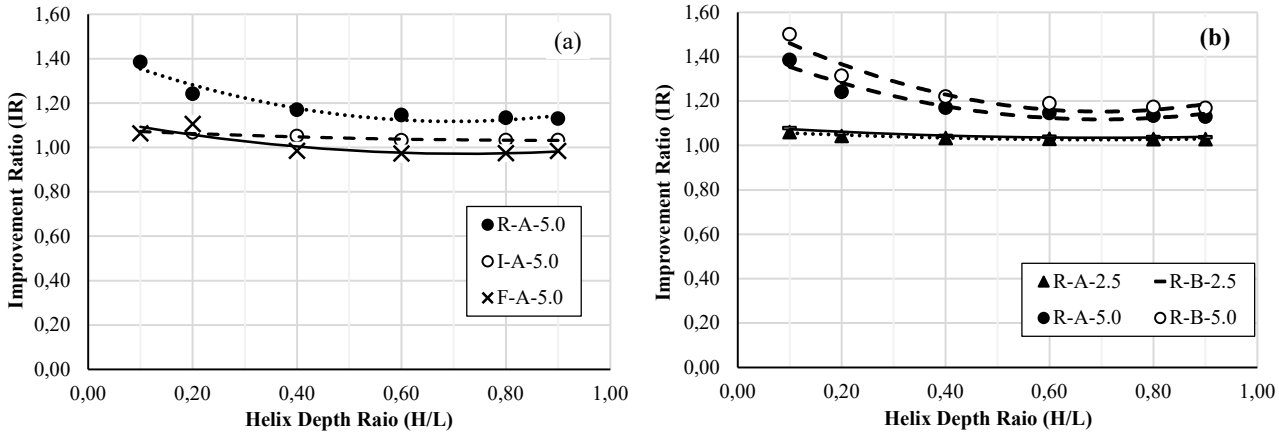

Fig. 3 Analytical results, lateral horizontal load: (a) Category "A", D/d = 5.0, (b) Category "A" and "B" D/d = 2.5 and 5.0

- The increase in both pile geometry, from category (A) to category (B), and helix diameter ratio (D/d), from 2.50 to 5.00, cause increasing in IR values. This is a general observation for any pile shaft rigidity and under any loading mode which is a direct result from (1), (2) and (12), for V > 0.
- With relatively small dimensions, i.e., geometrical category (A), under any loading mode, simultaneous or successive, the IR values of rigid piles are higher than those of flexible piles (i.e., Fig. 4 (b)). The same conclusion extends to geometrical category (B) for helices at H/L ≥ 0.40. This could be attributed to the large value of friction resistance Q_F for rigid piles relative to that for flexible piles. For large dimensions, category (B), the IR values of rigid piles are decreasing to values less than those of flexible piles, which is more obvious under the high level of vertical load (V = V2). There is a reduction in the resisting moment (M_h), due to the increase of V, which is more affecting ΔQ, for rigid piles, than δx^*, for flexible piles.
- The variations in the ratio (IR) to the helix depth ratio (H/L) show that high IRs are obtained with helices at H/L ≤ 0.40, except for rigid shafts with large geometries under heavy vertical loads. The best values of IR are mostly within 0.40 ≤ H/L ≤ 0.60 (i.e., Fig. 4 (c)).
- One of the unexpected results is that the improvement ratio of helical piles with flexible shaft rigidity increases when helices at H/L < 0.4 and decreases at H/L > 0.4 (i.e., for category B, Fig. 4 (d)).
- Under the action of BCLs, flexible models of helices at H/L < 0.40, gave higher values of IR than those obtained by the other models (i.e., Figs. 4 (c) and (d)).

III. Numerical Modelling

PLAXIS-3D-V20 is the FEM software used for numerical modelling in this study. Fig. 5 (a) presents the fine mesh discretisation used. The mesh dimensions were chosen to be large enough to eliminate boundary effects. Mohr–Coulomb criteria were used to model the soil. The execution effect was taken into consideration by adding a soil disturbance zone around the pile shaft (Fig. 5 (b)); its diameter was twice the diameter of the helix and extended to 0.10 meters below the helix level. The pile shaft was modelled as a volume of steel material and the helix as a plate element with 0.02 m thickness using steel linear nonporous material.

The soil–pile interaction was modelled as an interface element assigned to the pile model with a strength reduction factor ($R = \frac{\tan \varphi^*}{\tan \varphi} \approx 0{\cdot}7$) where φ^* is the sand–pile interface friction angle [17]. The model was verified two times to confirm its reliability. The first verification was done by modelling the previously conducted full-scale pile load test (PA-1) [22], and modelling the current laboratory loading tests.

Modelling Field Loading Test

The Normalised load-displacement relationships from field measurements [22] are presented in Fig. 6 and Table II. To prove the current numerical model results' validity. (δv) is vertical pile displacement, (V) is the vertical load and (d) is the pile shaft diameter. Results of field and numerical results show a good agreement.

Modelling the Laboratory Experimental Programme

This section details a laboratory investigation program for pile models of different helix locations along the pile length. Laboratory loading tests were conducted to verify the numerical model.

Testing Apparatus

Fig. 7 shows the testing apparatus, which was composed of a soil bin filled with sand (item 14), a pile model with a loading cap (item 8), a vertical loading system (items 1, 2, 3, 4, 6, 9, and 10), a horizontal loading system (items 11, 12 and 13), and displacement measuring dial gauges (items 5 and 7).

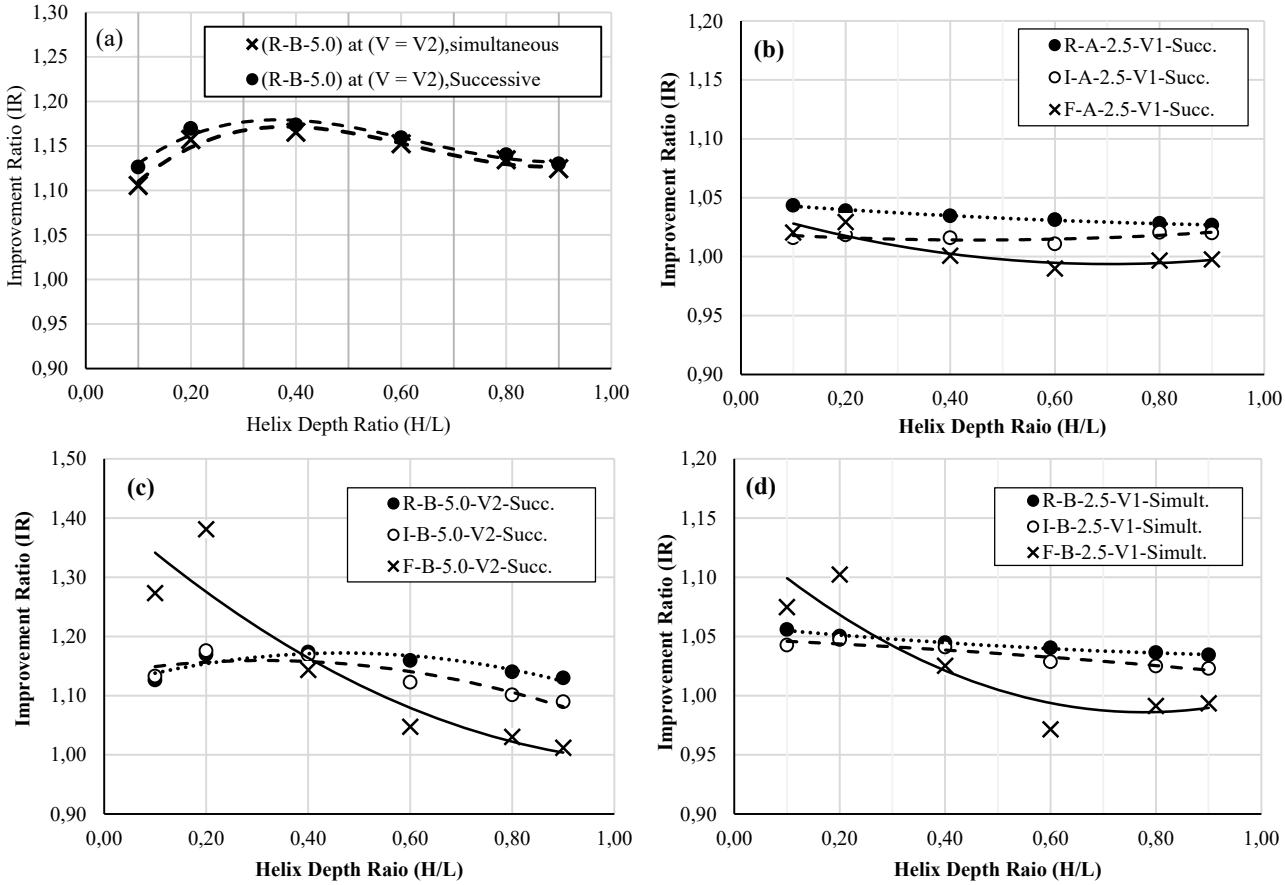

Fig. 4 Analytical results, BCLs: (a) Rigid model category "B", D/d = 5.0, (b) Category "A", D/d = 2.5, successive loading V = V1, (c) Category "B", D/d = 5.0, successive loading V = V2 and (d) Category "B", D/d = 2.5, simultaneous loading V = V1

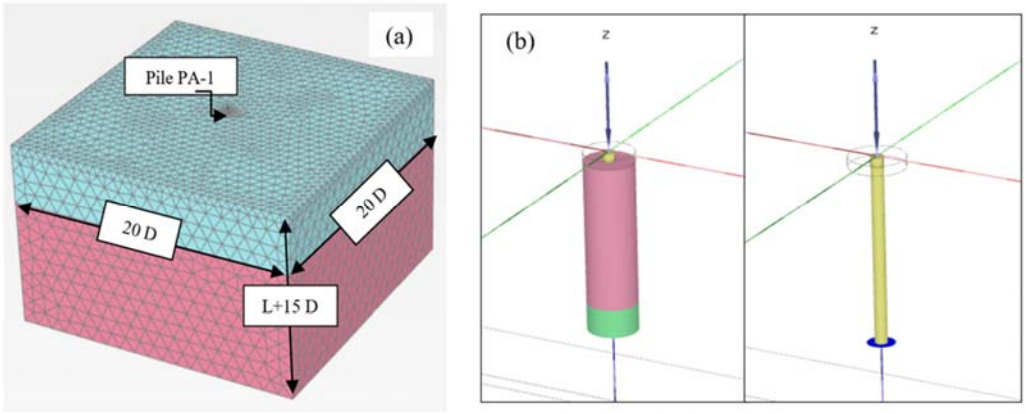

Fig. 5 The numerical model: (a) FE mesh used in the PLAXIS-3D, (b) Pile model, with and without soil disturbance zone

Soil Bin

The soil bin is a cylindrical steel tank with a sidewall 10 mm thick stiffened with 3-ring stiffeners. The tank base was of a rigid steel circular plate with a thickness 25 mm. The internal dimensions of the tank are 750 mm in diameter and 600 mm in height.

Testing Soil

The soil is a uniform SAND classified as SP or A-3 according to the USCS or AASHTO classification systems, respectively. The sand properties are listed in Table II. To fill the soil bin, four layers of sand were placed, each 150 mm thick and uniformly compacted by a hammer of 4 kg falling freely from a height of 300 mm. Due to grain uniformity, dry compaction cannot result in a relative density greater than 40%.

Pile Models

Six pile models were considered, PM-0 to PM-5. The model PM-0 is a conventional straight pile, whereas the others, PM-1 to PM-5, are helical pile models. The shapes and geometrical

properties of the pile models are presented in Fig. 8 and Table III. During each test, a rigid aluminium cap (50 × 50 × 20 mm) was affixed to the top of the pile to transfer test loads and to support the displacement measuring dial gauges.

TABLE II
SOIL AND PILE PROPERTIES FOR MODELLING THE FIELD TEST [22]

Properties	Soil Layers				Pile
	Sand 1 From depth 0.0 to 5.0		Sand 2 From depth 5.0 to 15		
	Disturbed	Un-disturbed	Disturbed	Un-disturbed	
Material Model	Mohr Columb	Mohr Columb	Mohr Columb	Mohr Columb	Linear Elastic
Drainage Type	Drained	Drained	Drained	Drained	Non-Porous
Unit weight, γ (kN/m^3)	18	20	18	20	78.5
Elastic modulus, E (MPa)	25	50	25	50	200 x10^3
Friction angle, φ^0	24	33	21	30	-
Dilatancy angle, Ψ^0	0.0	3.0	0.0	0.0	-
Cohesion, c (kPa)	0.0	0.0	0.0	0.0	-
Poisson's ratio, m	0.3	0.3	0.3	0.3	0.28

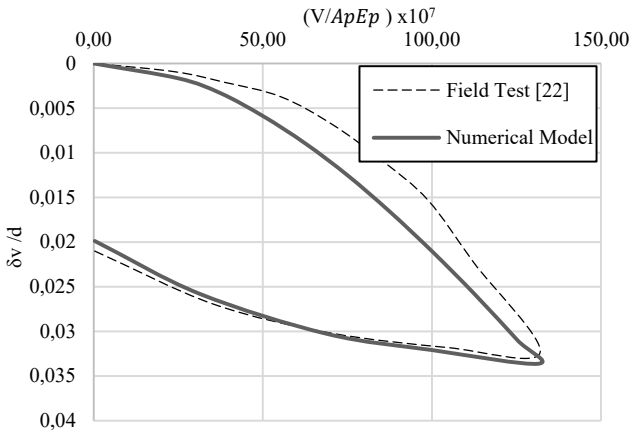

Fig. 6 Normalised load-displacement relationships for the field test [22], and the corresponding numerical model

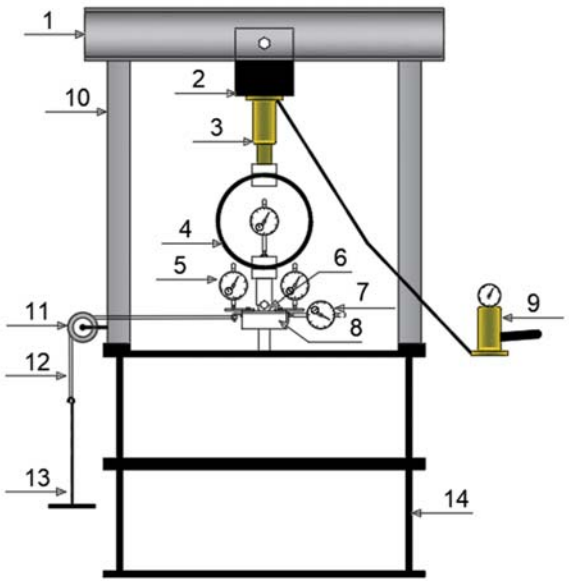

Fig. 7 Testing apparatus

TABLE III
GEOTECHNICAL PROPERTIES OF SAND

Property	Value	Specification ASTM
Minimum dry unit weight, (kN/m^3)	1.56	D-1557
Maximum dry unit weight, (kN/m^3)	1.72	D-1557
Specific Gravity, Gs	2.65	D-854
Coefficient of curvature, Cc	0.57	D-422
Coefficient of uniformity, Cu	1.056	D-422
Properties at Dr=40%		
Angle of internal friction, ϕ (°)	33.7	D3040-04
Dry unit weight, γ (kN/m^3)	1.62	

TABLE IV
GEOMETRICAL PROPERTIES OF THE HELICAL PILE MODELS USED IN THE EXPERIMENTAL PROGRAMME

General geometrical properties	Dimension
Total length (L_o)	600 mm
Embedded length in soil (L)	500 mm
Free height (Y)	100 mm
Pile shaft diameter (d)	20 mm
Helix diameter (D)	50 mm
Helix diameter ratio (D/d)	2.5
Number of helices	1
Thickness of the helix	2.0 mm
Pitch of helix (P)	20 mm

Model	PM-0	PM-1	PM-2	PM-3	PM-4	PM-5
H/L	----	0.90	0.80	0.60	0.40	0.20

Loading Systems

The BCLs are vertical compression and horizontal loads, which act successively at the pile head. As shown in Fig. 7, the vertical loading system was composed of a loading frame (items 1, 2, and 10), a hydraulic jack with a 50 kN maximum capacity (items 3 and 9), a proving ring with a 2 kN maximum capacity (item 4) and a loading arm with a roller end (item 6). The horizontal loading system consisted of a steel wire (item 12), a weight hanger (item 13) and a pulley (item 11).

Displacement Measuring System

Under the action of the BCL$_S$, the pile head was displaced vertically and horizontally. Vertical displacements were measured by two vertical dial gauges with an accuracy of 0.01

mm (item 5), while the corresponding horizontal displacements were measured by a horizontal dial gauge with an accuracy of 0.01 mm (item 7).

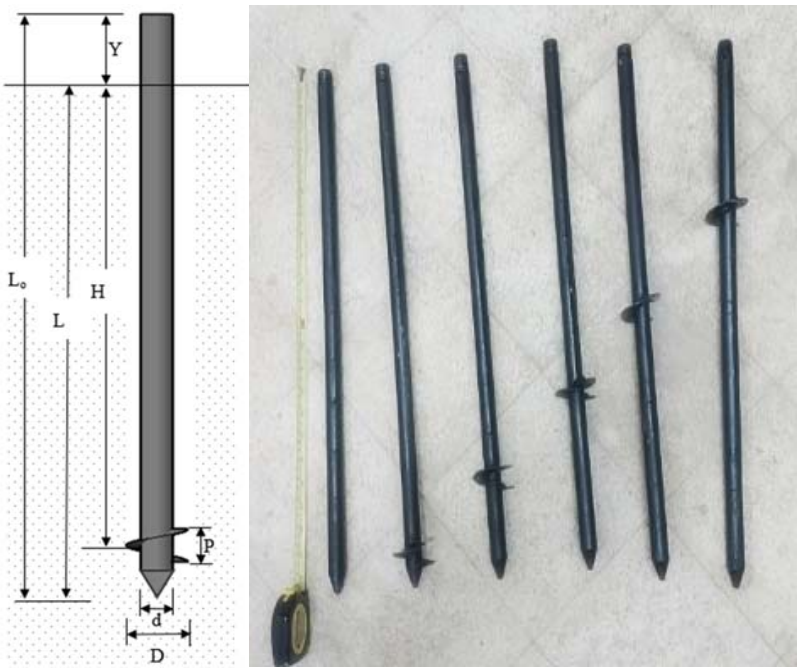

Fig. 8 Geometry of the helical pile models and the conventional pile

Test Preparation

The main issue of test preparation was how to insert the pile model into the soil bed. As lab work, the model insertion could be performed either by boring or by pre-replacement. In the boring method, the soil bed was first prepared, and then the pile was mechanically drilled using a low-speed hand electric driller. During drilling, a suitable guiding system was used to determine the location and verticality of the drilled pile. In the pre-replacement method, the pile was first hung and placed in the required location at the centre of the soil bin, after which the soil bed was placed and compacted around the pile. Following pile insertion, the cap was affixed to the pile's top, and the measurement devices for the loads and displacements were adjusted.

Testing Programme

The testing programme consisted of 16 tests in three groups (Fig. 9). Group (1) represents the case of horizontal loading only, whereas groups (2) and (3) represent the cases of BCLs. In the BCL_S groups, the vertical load was first gradually increased from 0.00 to the required V, after which the horizontal loading started. These loading sequences correspond to successive BCLs conditions. The chosen vertical loads were assumed as V1 and V2 where V2 = 0.45 kN is approximately 0.85 to 0.90 of the ultimate bearing loads (Vult conv.) for the pile model PM-0 (conventional), which is considered the load corresponding to a vertical displacement of 10% of the pile shaft diameter (d) i.e. δv /d=0.1 [31], (Fig. 10), while V1 = 0.50 V2 = 0.225 kN.

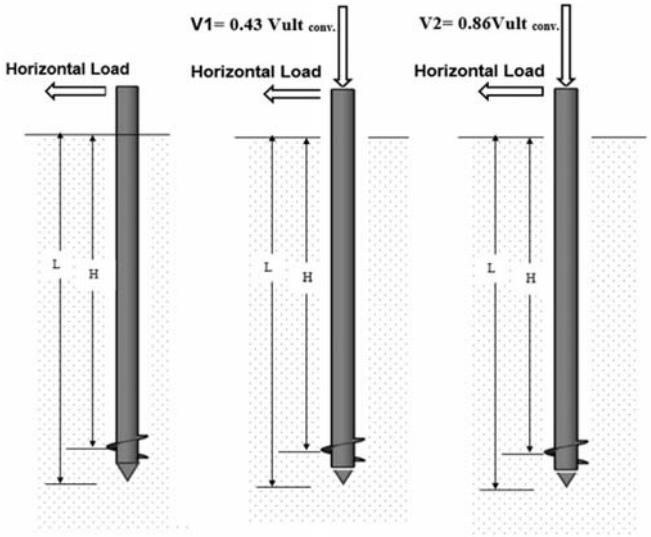

Fig. 9 Testing programme on single helical pile

The dimensions of the modelled piles are shown in Table IV. Pile material and Soil properties are presented in Table V. Fig. 11 illustrates a sample of the relationship between the normalised load-displacement curve of the experimental results and the calibrated FEM model for a single helical pile (PM-2) under horizontal loading and combined loading which confirms the reliability of the numerical model.

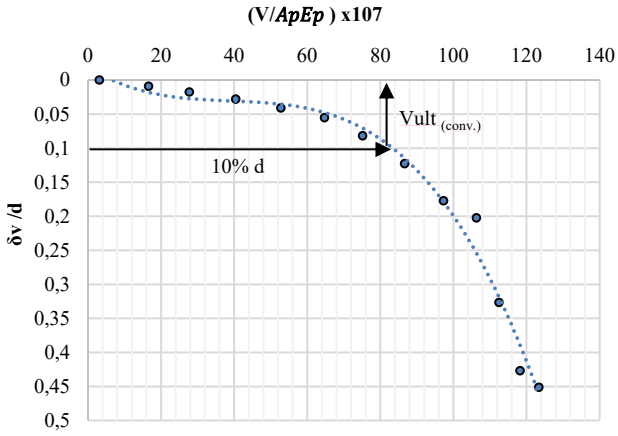

Fig. 10 Experimental results, Normalised vertical load–vertical displacement relationship

TABLE V
SOIL AND PILE PROPERTIES FOR NUMERICAL MODELLING OF LABORATORY TESTS

Properties	Soil	Pile
Material Model	Mohr Columb	Linear Elastic
Drainage Type	Drained	Non-Porous
Unit weight, γ(kN/m^3)	15.9	78.5
Elastic modulus, E (kN/m^2)	40000	200 x 10^6
Friction angle, φ^0	33	-
Dilatancy angle, Ψ^0	3	-
Cohesion, c (Kpa)	0.1	-
Poisson's ratio, μ	0.3	0.28

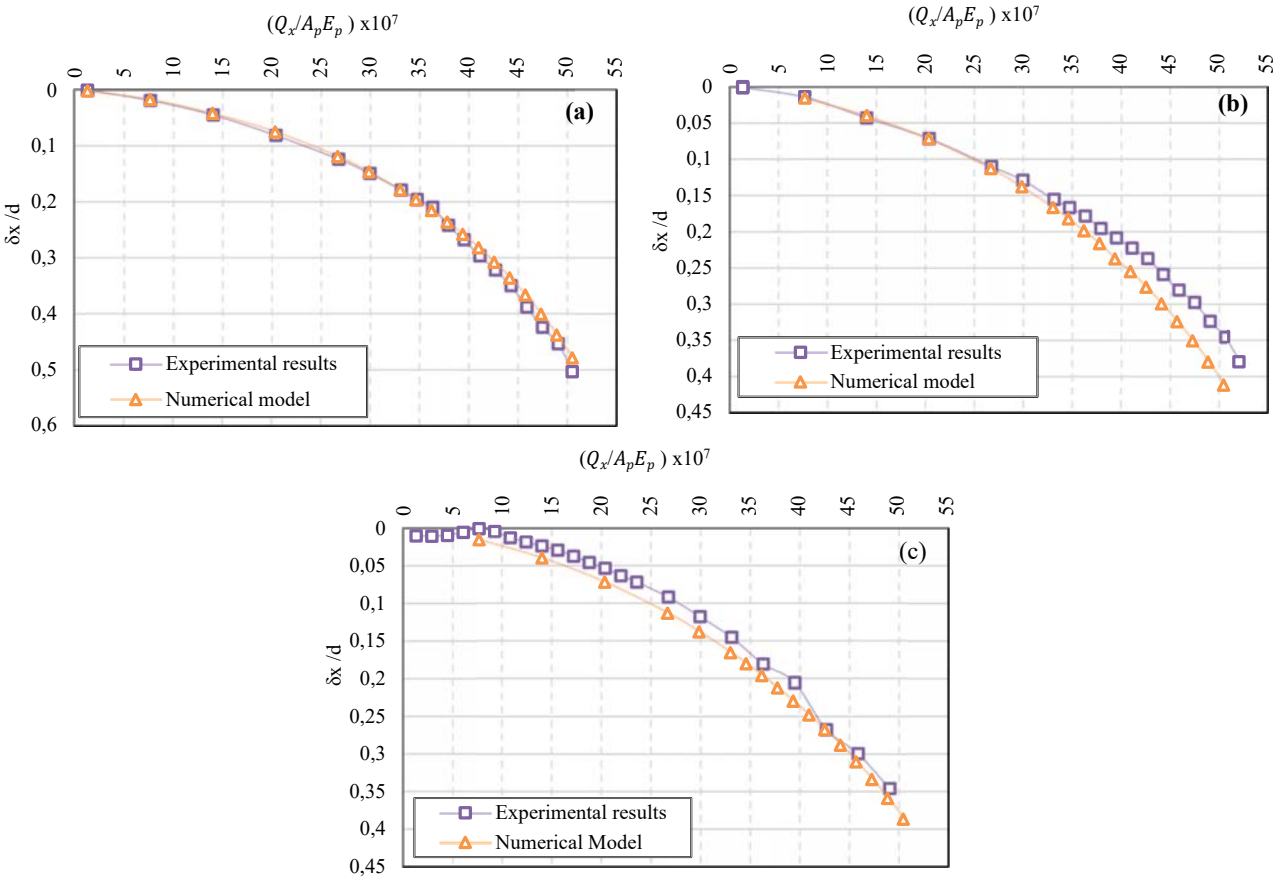

Fig. 11 Normalised load–load-displacement relationships for the laboratory tests on the pile model (PM-2) and the corresponding numerical models, (a) Group-1 (b) Group-2 (c) Group-3

Numerical Model Results and Discussion

Based on the proven reliability of the considered PLAXIS-3D model, a detailed parametric study was conducted, using helical pile models as those used in the analytical model applications, Table I. The soil and pile material properties are presented in Table V, where the angle of internal friction (φ) and the unit weight (γ) were based on laboratory measurements. Tops and tips of the pile's shafts are fitted by 0.025 m steel plates.

Lateral Horizontal Load (V = 0)

Fig. 12 shows the created total displacement contour in the soil around the helical pile while laterally loaded. The figure signifies the effect of changing the rigidity from flexible to rigid shafts for two models of piles, R-B-5.0 and F-B-5.0, having the same pile shaft diameter (d). Also, Fig. 13 shows the variations

in the improvement ratio (IR) against the helix depth ratio (H/L) due to the action of the horizontal load only. The effect of the pile shaft rigidity, pile geometry, and helix diameter ratio (D/d) are investigated. The following were observed:

- In general, the presence of helices improved the lateral resistance of all helical pile models with rigid and intermediate rigidity, i.e., IR > 1.00 even if the helix is deep (Fig. 12 (a)). For helical piles with flexible shaft rigidity (IR > 1.00) is only at H/L < 0.4 but for helix below H/L = 0.4, there is no effect in lateral performance.
- Changing the rigidity condition from R to I to F decreases the overall value of IR.
- Geometry was significantly affecting the behaviour of helical piles of rigid and intermediate shaft rigidities but mostly does not influence the behaviour of helical piles of flexible pile shaft rigidity. The largest effect corresponds to rigid shafts, where the IR increases with increasing pile geometry from model (A) to model (B) (Fig. 13 (c)).

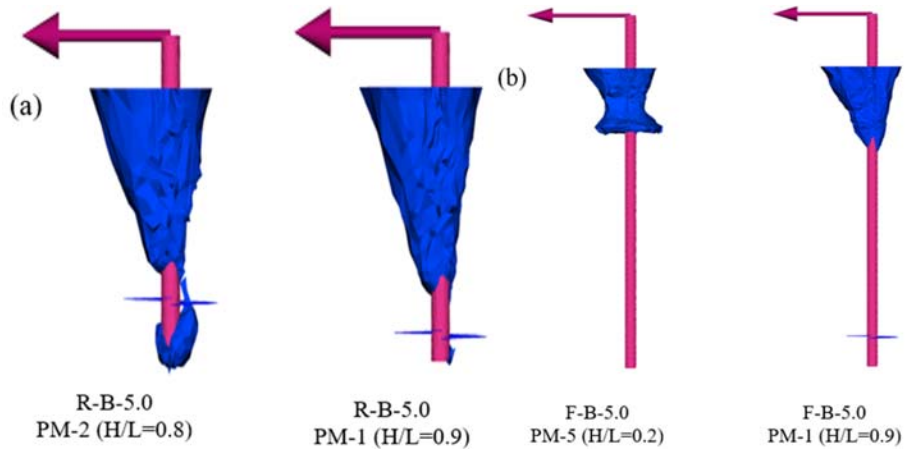

Fig. 12 Total displacement contour - horizontal loading: (a) Rigid shaft rigidity Category "B", D/d = 5.0 and (b) Flexible shaft rigidity Category "B", D/d = 5.0

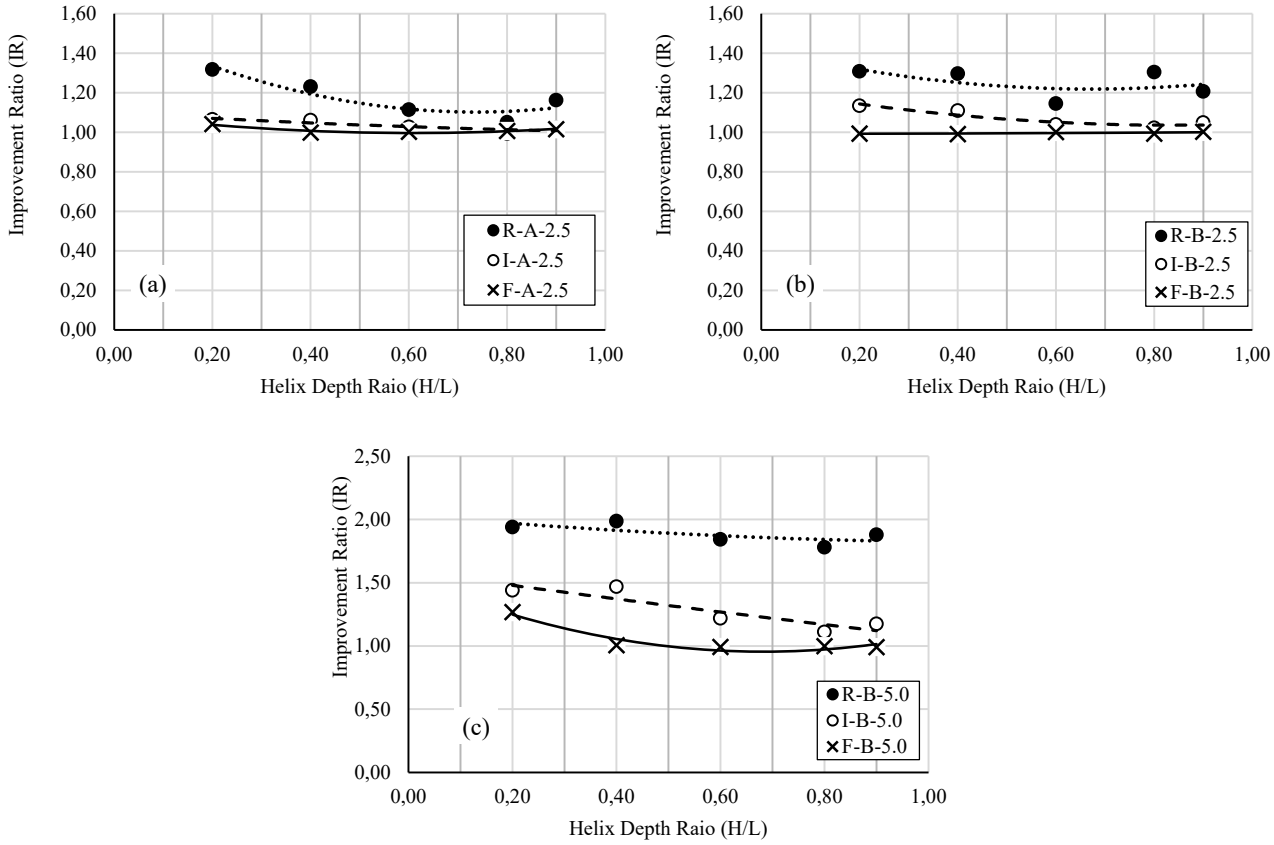

Fig. 13 Numerical results, horizontal loading: (a) Category "A", D/d = 2.5, (b) Category "B", D/d = 2.5, (c) Category "B", D/d = 5.0

Bearing Combined Loads

The influence of BCLs was examined by applying different values of vertical displacement (δv), at the pile head, to represent the acting vertical load (V). Vertical displacements as δv = 2.5%D and δv = 4.0%D were presented the action of vertical loads, V = V1 and V = V2, respectively. The two values of displacements were applied simultaneously and successively with lateral displacements (δx), by which the limit resultant displacements be δr = 10%D.

Figs. 14-16 present the variations in the improvement ratio (IR) vs. the change in the helix depth ratio (H/L) due to the action of BCLs, considering the effects of pile shaft rigidity, geometrical category, helix diameter ratio (D/d), and loading mode, simultaneous and successive. In addition, the displacement fields around the pile shafts of the pile models, F-B-5.0, I-B-5.0 and R-B-5.0 are presented in Figs. 17-25. The displacement fields present the vectors of the resultant displacements (δr) around the pile shafts to help in explaining the observed behaviours of the considered helical piles. The following observations were assembled:

- The improvement ratios (IR) were increased with increasing helix diameter ratio (D/d) and decreasing helix depth ratio (H/L). These observations were valid for all pile models, except for flexible piles with helices at H/L ≥ 0.60. With these exceptional models, the IR values were insignificantly affected by the variations of D/d and H/L, Figs. 15 (a) and (b). This behaviour is compatible with that observed by the analytical model, as discussed in section 2.4.1. According to the displacement fields shown in Fig. 17, H/L = 0.90, the resultant displacement vectors around the helices are almost zero or only vertical which means that it does not affect the lateral resistance of the pile.
- For helical piles of rigid shafts, the IR values increased with increasing vertical load. For intermediate models, the IR values were increased under the action of the low vertical load (V = V1) and decreased relatively under the action of the high vertical load (V = V2), but still IR > 1.00. For flexible models of helices, at H/L ≤ 0.60, the performance of the model worsened with increasing vertical load, where the IR values decreased to less than 1.00. As observed in Figs. 17 (d)-(f), large vertical displacement vectors are there around the helices which may correspond to a local soil failure around the helix. This could explain the observed reduction in IR values.

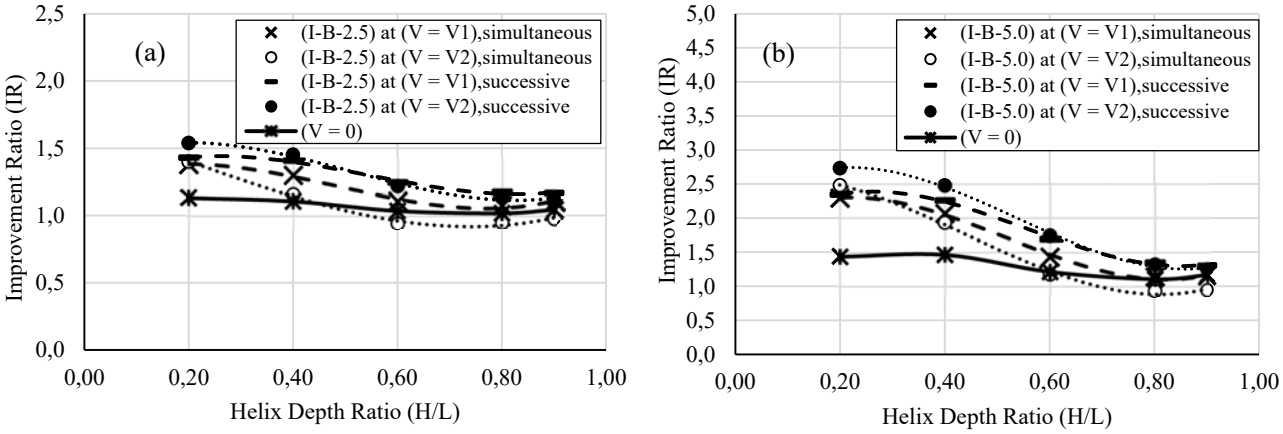

Fig. 14 Numerical results, BCLs, and intermediate models, for successive and simultaneous loadings, Category "B", D/d =2.5 and 5.0

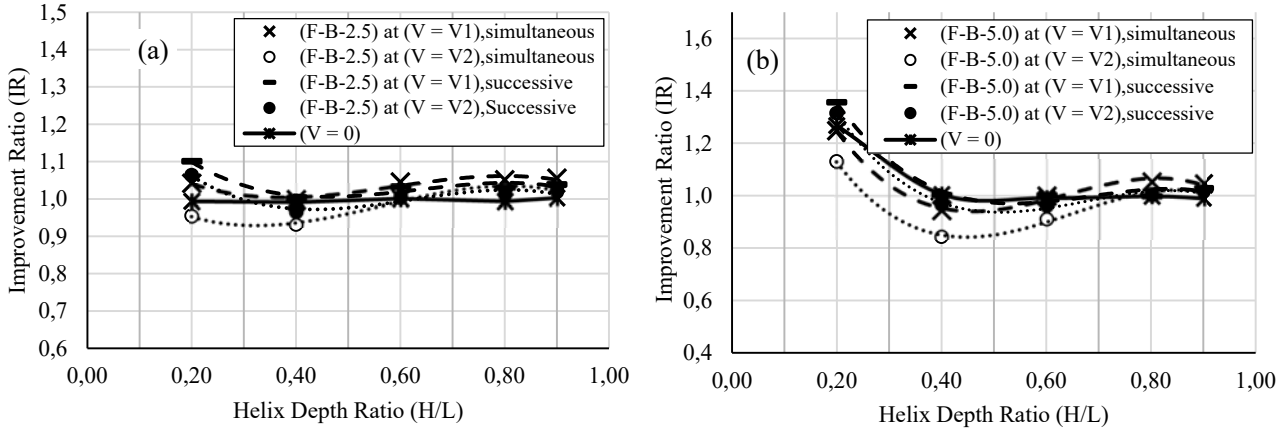

Fig. 15 Numerical results, BCLs, and flexible models for successive and simultaneous loadings, Category "B", D/d = 5.0

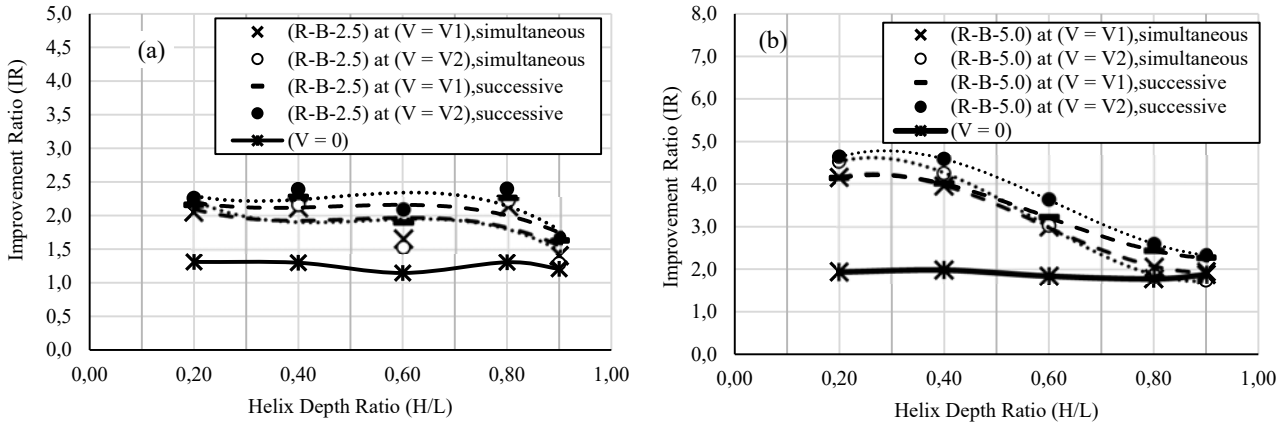

Fig. 16 Numerical results, BCLs, and rigid models, for successive and simultaneous loadings, Category "B", D/d = 5.0

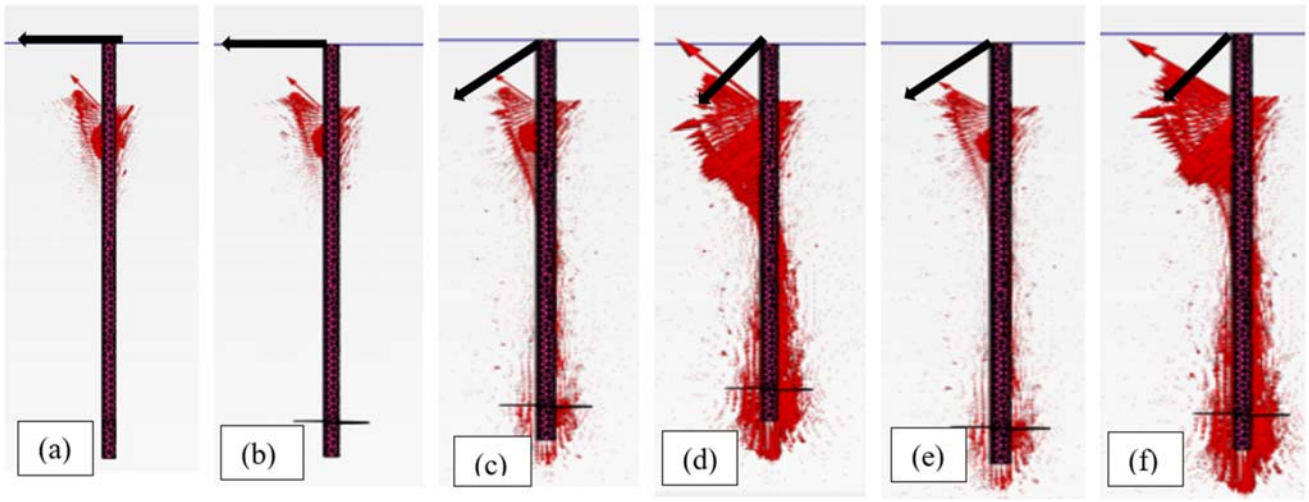

Fig. 17 Numerical resultant displacement results for the conventional pile and model "F-B-5.0" at (H/L = 0.9) in different loading conditions, the conventional pile in horizontal loading, (b) "F-B-5.0" in horizontal loading, (c) "F-B-5.0" in BCLs (V1) simultaneous loading, (d) "F-B-5.0" in BCLs (V2) simultaneous loading, (e) "F-B-5.0" in BCLs (V1) successive loading and (f) "F-B-5.0" in BCLs (V2) successive loading

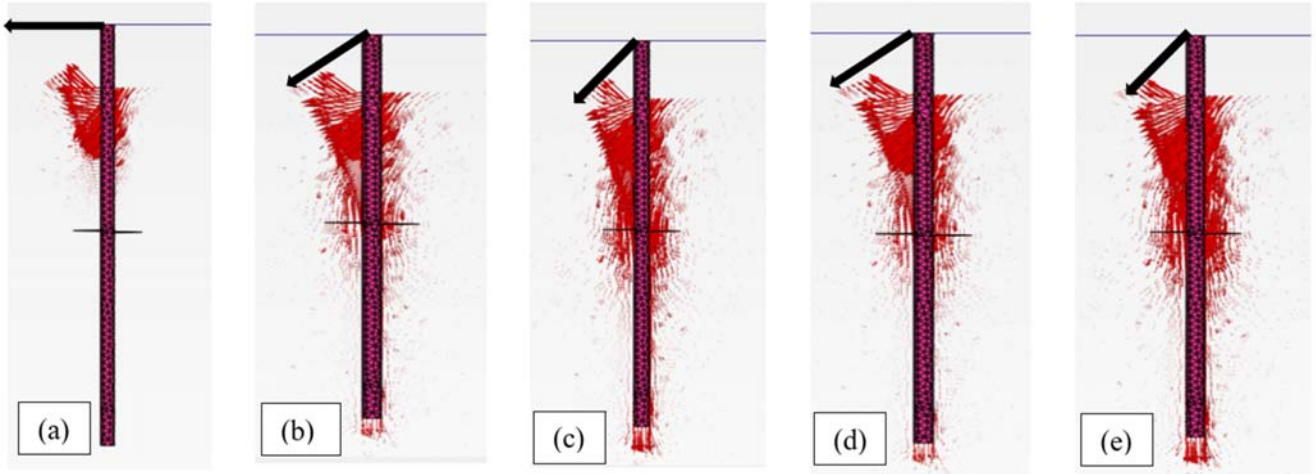

Fig. 18 Numerical resultant displacement results for model "F-B-5.0" at (H/L = 0.4) in different loading conditions, (a) "horizontal loading, (b) BCLs (V1) simultaneous loading, (c) BCLs (V2) simultaneous loading, (d) BCLs (V1) successive loading and (e) BCLs (V2) successive loading

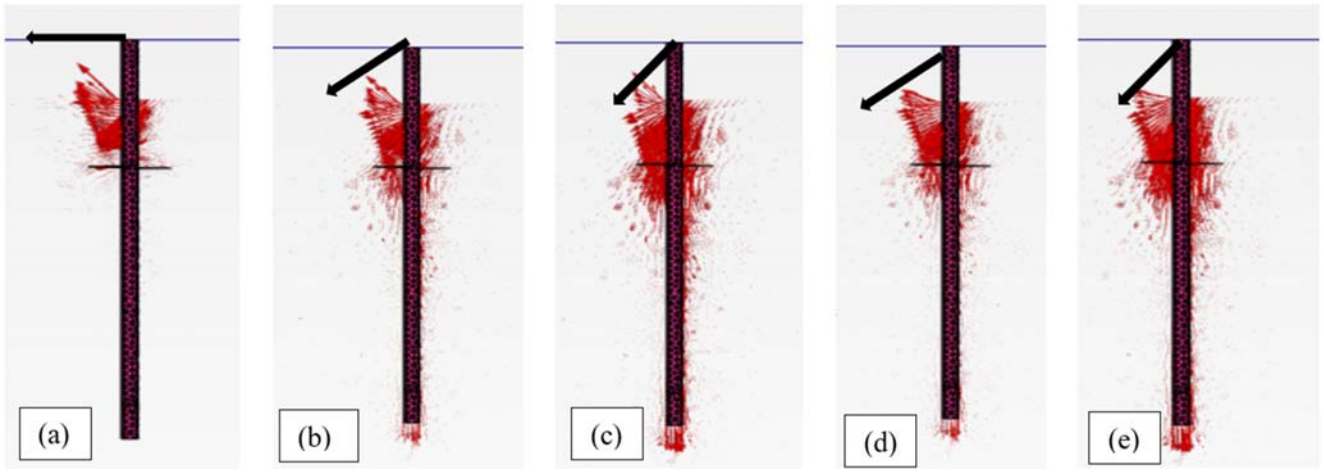

Fig. 19 Numerical resultant displacement results for model "F-B-5.0" at (H/L = 0.2) in different loading conditions, (a) horizontal loading, (b) BCLs (V1) simultaneous loading, (c) BCLs (V2) simultaneous loading, (d) BCLs (V1) successive loading and (e) BCLs (V2) successive loading

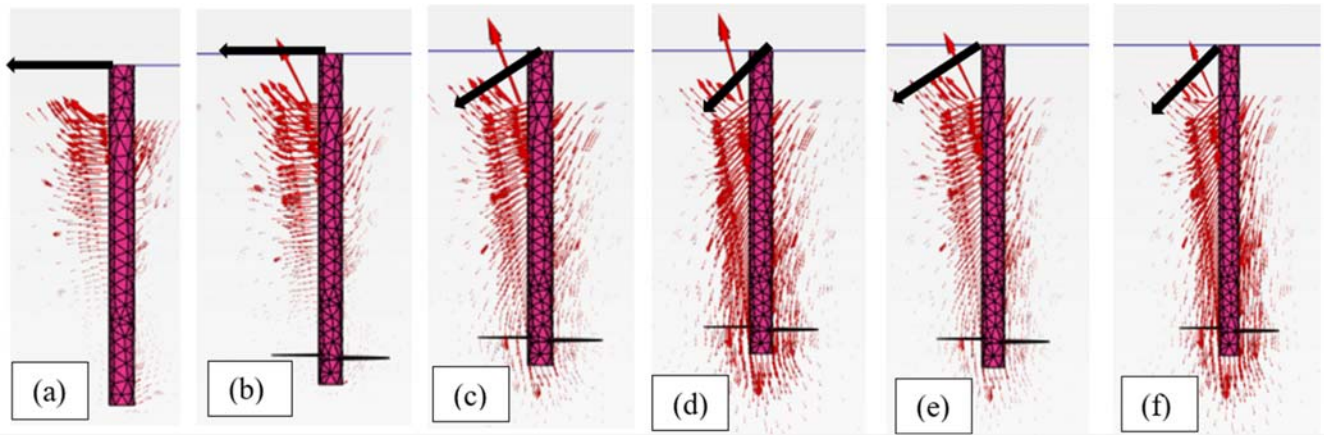

Fig. 20 Numerical resultant displacement results for the conventional pile and model "I-B-5.0" at (H/L = 0.9) in different loading conditions, the conventional pile in horizontal loading, (b) "I-B-5.0" in horizontal loading, (c) "I-B-5.0" in BCLs (V1) simultaneous loading, (d) "I-B-5.0" in BCLs (V2) simultaneous loading, (e) "F-A-5.0" in BCLs (V1) successive loading and (f) "I-B-5.0" in BCLs (V2) successive loading

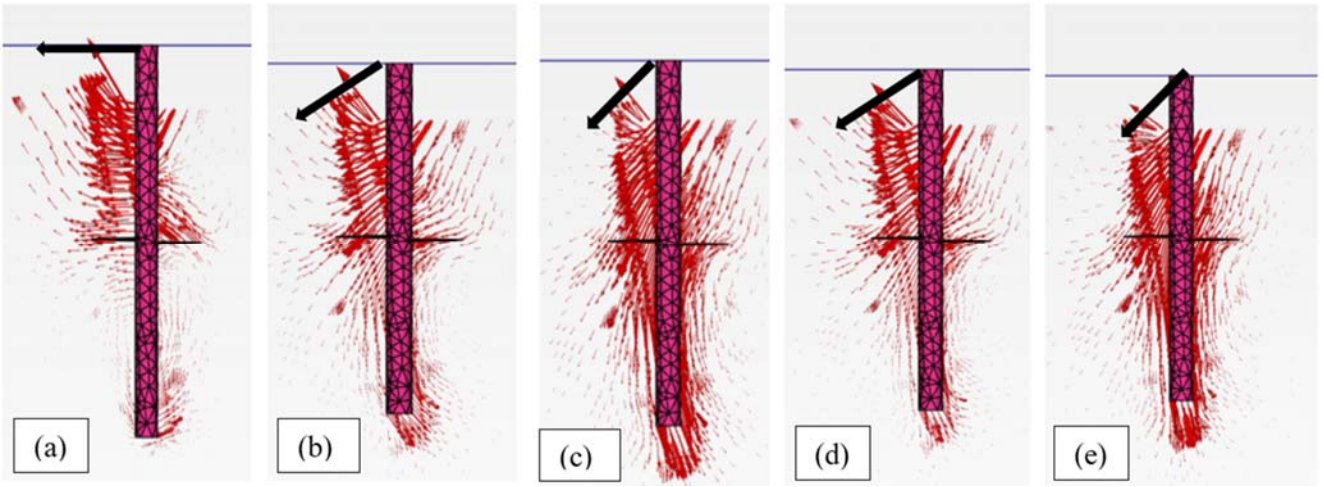

Fig. 21 Numerical resultant displacement results for model "I-B-5.0" at (H/L = 0.4) in different loading conditions, (a) horizontal loading, (b) BCLs (V1) simultaneous loading, (c) BCLs (V2) simultaneous loading, (d) BCLs (V1) successive loading and (e) BCLs (V2) successive loading

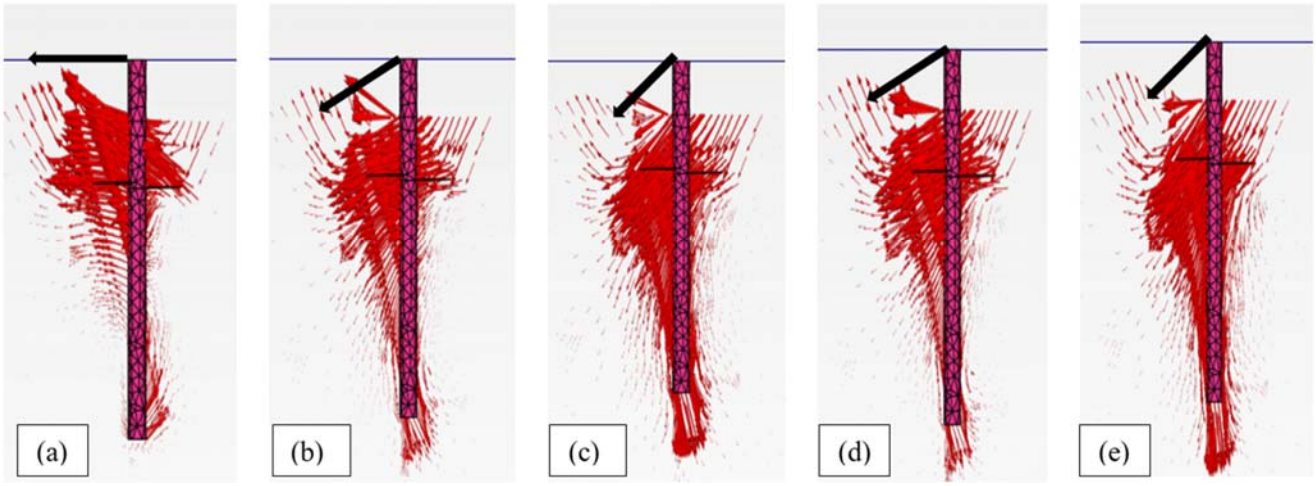

Fig. 22 Numerical resultant displacement results for model "I-B-5.0" at (H/L = 0.2) in different loading conditions, (a) horizontal loading, (b) BCLs (V1) simultaneous loading, (c) BCLs (V2) simultaneous loading, (d) BCLs (V1) successive loading and (e) BCLs (V2) successive loading

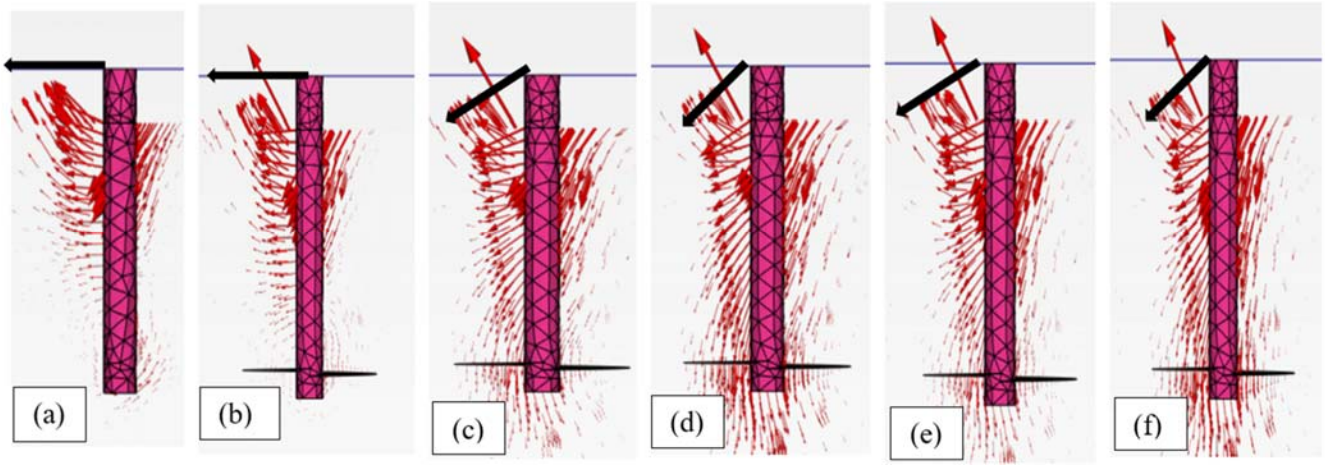

Fig. 23 Numerical resultant displacement results for the conventional pile and model "R-B-5.0" at (H/L = 0.9) in different loading conditions, the conventional pile in horizontal loading, (b) "R-B-5.0" in horizontal loading, (c) "R-B-5.0" in BCLs (V1) simultaneous loading, (d) "R-B-5.0" in BCLs (V2) simultaneous loading, (e) "F-A-5. 0" in BCLs (V1) successive loading and (f) "R-B-5.0" in BCLs (V2) successive loading

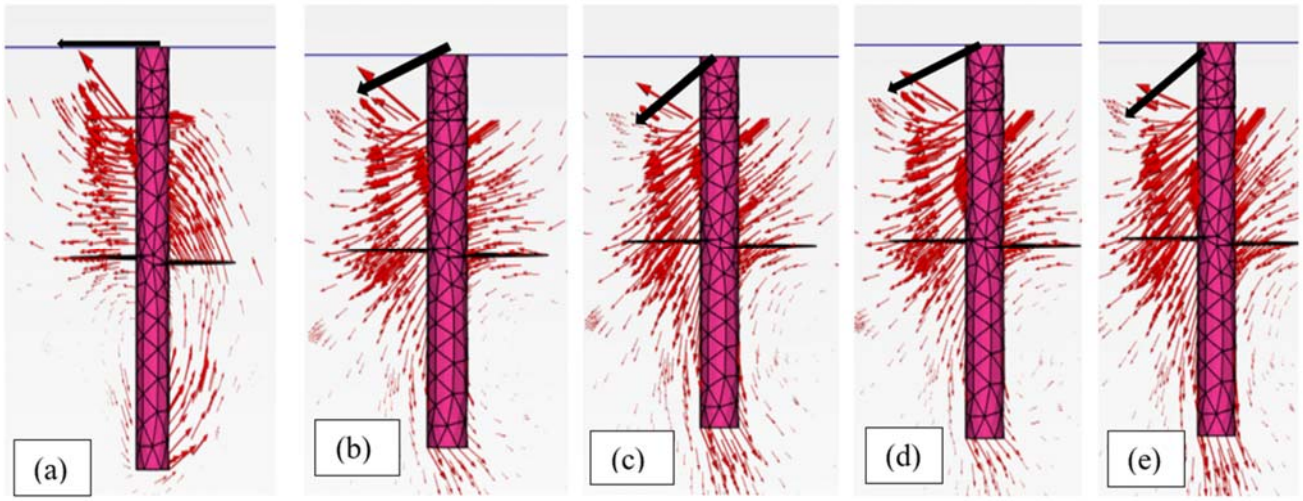

Fig. 24 Numerical resultant displacement results for model "R-B-5.0" at (H/L = 0.4) in different loading conditions, (a) "horizontal loading, (b) BCLs (V1) simultaneous loading, (c) BCLs (V2) simultaneous loading, (d) BCLs (V1) successive loading and (e) BCLs (V2) successive loading

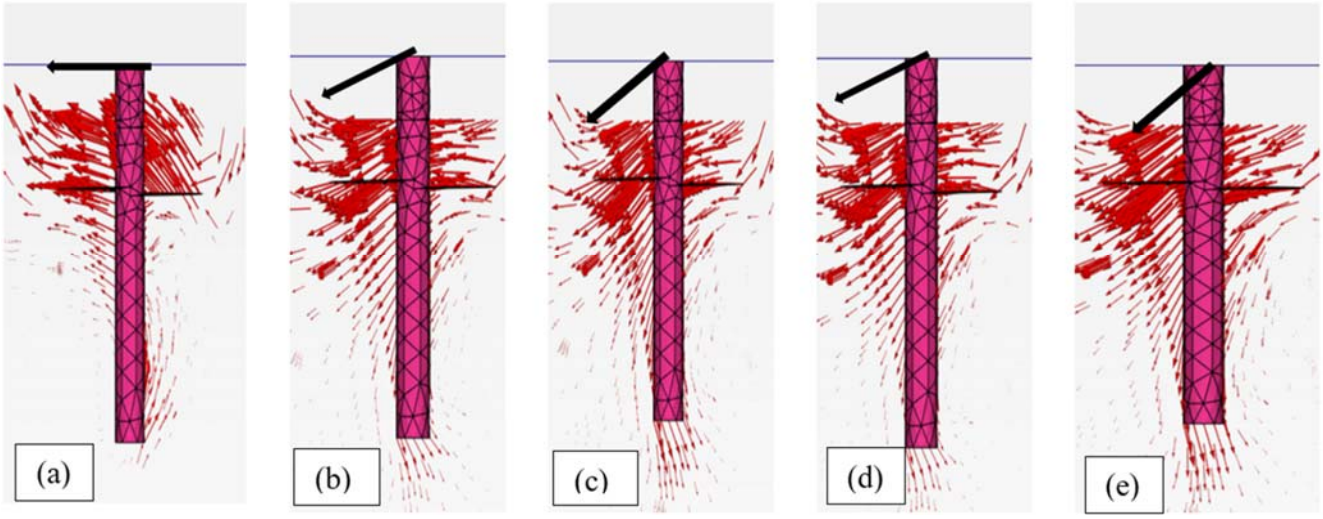

Fig. 25 Numerical resultant displacement results for model "R-B-5.0" at (H/L = 0.2) in different loading conditions, (a) "horizontal loading, (b) BCLs (V1) simultaneous loading, (c) BCLs (V2) simultaneous loading, (d) BCLs (V1) successive loading and (e) BCLs (V2) successive loading

- Changing the BCLs mode from simultaneous to successive caused a rise in the IR values, which increase with the increase in pile geometrical category, from (A) to (B), and with the increase in helix diameter ratio (D/d), from 2.50 to 5.00. Referring to Figs. 17-25, under successive mode, the displacement victors around the pile shafts and helices became close to vertical direction which means that the soil became denser before starting the action of horizontal loading and then the lateral resistance increased.

IV. Conclusions

The behaviour of helical piles under BCLs has been investigated. Through three stages—analytical, experimental, and numerical—this study involved a trial to answer questions about the effects of factors such as the pile geometry, relative rigidity of the pile shaft, and loading pattern on the behaviour of helical piles subjected to BCLs. Analytically, the lateral resistance of a helical pile was assumed to be the sum of three components: horizontal friction between the helix plate and the soil below it, bearing resistance between the helix plate and the surrounding soil, and lateral resistance of the pile shaft without a helix. Experimentally, a set of 16 laboratory tests was conducted on five helical pile models with different helices depths in the purpose of the numerical verification. Numerically, a three-dimensional FE model was prepared with PLAXIS-3D software. The reliability of the proposed model was verified and confirmed twice, once by modelling a previously conducted field pile load test and the second by modelling the conducted laboratory tests. The behaviour-wise likeness was mostly between the analytical and numerical observations. In general, the behaviour of helical piles under BCLs condition was significantly affected by the pile geometry, shaft rigidity and loading pattern but in a highly interacted manner, as subsequently concluded:

- Increasing the pile geometry improves the pile performance, i.e., higher IR ratio, especially for piles with rigid and intermediate shaft rigidity.
- An increase in shaft rigidity, from flexible to intermediate to rigid, improves the pile performance, i.e., the best performance is for helical piles of rigid shafts with feasible construction limits.
- Within the limits of the study, helices with D/d = 5.0 at H/L ≤ 0.60, perform the best for all modes of loading.
- The presence of a vertical bearing load (V > 0.00) improves the performance of piles with rigid or intermediate rigidity, in contrary for flexible shafts. The pile performance degrades at the high level of vertical loads in which the vertical load becomes very close to the ultimate value.
- Analytical and numerical models are both confirming the positive effect of changing the BCLs mode, from simultaneous to successive, on the behaviour of helical piles of rigid shafts. The influence is quite clear by numerical analysis; however, the analytical analysis shows this influence for piles with rigid shafts.
- Effect of vertical loading is obvious at H/L < 0.6 for rigid and intermediate shafts.
- If the pile was designed to resist bearing loads and the helix is deep (H/L > 0.4), it could resist an extra lateral load if its shaft rigidity rigid or intermediate. This increase could be enhanced by applying vertical load which causes vertical displacement about 2.5-4% D.

Declaration of Interests

The authors declare that they have no known competing financial interests or personal relationships that could have appeared to influence the work reported in this paper.

Acknowledgments

Grateful acknowledgments to all individuals who contributed to the research, even if they did not meet the criteria for authorship. A special note of appreciation goes to Professor Yosra S.R. Elnaggar, Head of the International Publishing &

Nanotechnology Consultation Center (INCC) at PUA, for her valuable assistance in the international publishing process.

REFERENCES

[1] Pavan Kumar, P.V., et al., *Behaviour of Screw Pile Under Axial Compressive and Lateral Loading in Sand for Offshore Energy Foundations.* Advances in Offshore Geotechnics. Lecture Notes in Civil Engineering, 2020. 92: p. 393-403. https://link.springer.com/content/pdf/10.1007%2F978-981-15-6832-9_23.pdf.

[2] Sakr, M., *Lateral resistance of helical piles in oil sands*, in *Contemporary Topics in Deep Foundations*. 2009. p. 464-471. https://ascelibrary.org/doi/abs/10.1061/41021(335)58.

[3] Byrne, B.W., et al., *Helical piles: an innovative foundation design option for offshore wind turbines.* Philos Trans A Math Phys Eng Sci, 2015. 373(2035). https://www.ncbi.nlm.nih.gov/pubmed/25583860.

[4] Akl, S.A.Y., et al., *Lateral Performance of Helical Piles as Foundations for Offshore Wind Farms.* 2016: p. 449-458. https://ascelibrary.org/doi/abs/10.1061/9780784480137.043.

[5] Haldar, S., et al., *Advances in Offshore Geotechnics*, in *Challenges in the Design and Construction of Offshore Wind Turbine Foundations Including Sites in Seismic Areas*, S. Haldar, S. Patra, and R.K. Ghanekar, Editors. 2019. https://doi.org/10.1007/978-981-15-6832-9.

[6] Ullah, S.N., et al., *A Green Foundation for Offshore Wind Energy - Helical Piles*, in *World Engineering Convention, WEC2019*. 2019: Melbourne, Australia.

[7] McCartney, J.S., et al., *Review of torque models for offshore helical piles.* E3S Web of Conferences, 2020. 205: p. 12007. https://www.e3s-conferences.org/articles/e3sconf/abs/2020/65/e3sconf_icegt2020_12007/e3sconf_icegt2020_12007.html.

[8] Spagnoli, G., et al. *Helical piles as a novel foundation system for offshore piled facilities*. in *Abu Dhabi International Petroleum Exhibition and Conference*. 2015. SPE. https://onepetro.org/SPEADIP/proceedings-abstract/15ADIP/2-15ADIP/179935.

[9] Elkasabgy, M., et al., *Lateral Performance and p-y Curves for Large-Capacity Helical Piles Installed in Clayey Glacial Deposit.* Journal of Geotechnical and Geoenvironmental Engineering, 2019. 145(10): p. 04019078. https://ascelibrary.org/doi/abs/10.1061/%28ASCE%29GT.1943-5606.0002063.

[10] Sakr, M., *Performance of laterally loaded helical piles in clayey soils established from field experience.* DFI Journal - The Journal of the Deep Foundations Institute, 2018. 12(1): p. 28-41. https://doi.org/10.1080/19375247.2018.1430481.

[11] Elkasabgy, M., et al., *Lateral Vibration of Helical and Driven Steel Piles Installed in Clayey Soil.* Journal of Geotechnical and Geoenvironmental Engineering, 2018. 144(9): p. 06018009. https://ascelibrary.org/doi/full/10.1061/(ASCE)GT.1943-5606.0001899.

[12] Abdelghany, Y., et al. *Full-scale experimental and numerical analysis of instrumented helical screw piles under axial and lateral monotonic and cyclic loadings-A promising solution for seismic retrofitting*. in *ASCE IECC6 6th International Engineering and Construction Conference*. 2010. https://www.uwo.ca/engin/grcmembers/pdf/GRC_Report_No_GEOT-10-04.pdf.

[13] Mittal, S., et al., *Static Equilibrium of Screw Anchor Pile Under Lateral Load in Sands.* Geotechnical and Geological Engineering, 2010. 28(5): p. 717-725. https://link.springer.com/article/10.1007/s10706-010-9342-4.

[14] Abdrabbo, F.M., et al., *Laterally loaded helical piles in sand.* Alexandria Engineering Journal, 2016. 55(4): p. 3239-3245. https://www.sciencedirect.com/science/article/pii/S1110016816302319.

[15] Al-Neami, M.A., et al., *The influence of pile groups configuration on its stability in dry sand under lateral loads.* IOP Conference Series: Materials Science and Engineering, 2019. 579(1): p. 012043. https://dx.doi.org/10.1088/1757-899X/579/1/012043.

[16] Dave, S., et al., *Model Tests to Determine Lateral Load Capacity of Helical Piles Embedded in Sand.* 2019. 29: p. 529-538. https://link.springer.com/chapter/10.1007/978-981-13-6713-7_42.

[17] Al-Baghdadi, T.A., et al., *Effects of vertical loading on lateral screw pile performance.* Proceedings of the Institution of Civil Engineers - Geotechnical Engineering, 2017. 170(3): p. 259-272. https://doi.org/10.1680/jgeen.16.00114.

[18] Pavan Kumar, P.V., et al. *3D Numerical Analysis of Screw Pile Subjected to Axial Compressive and Lateral Load*. in *Soil Dynamics, Earthquake and Computational Geotechnical Engineering*. 2023. Singapore: Springer Nature Singapore. https://doi.org/10.1007/978-981-19-6998-0_8.

[19] Garakani, A.A., et al. *Load Capacity of Helical Piles with Different Geometrical Aspects in Sandy and Clayey Soils: A Numerical Study*. 2020. Cham: Springer International Publishing. https://link.springer.com/chapter/10.1007/978-3-030-34178-7_7.

[20] Nowkandeh, M.J., et al., *Numerical study of single helical piles and helical pile groups under compressive loading in cohesive and cohesionless soils.* Bulletin of Engineering Geology and the Environment, 2021. 80(5): p. 4001-4023. https://doi.org/10.1007/s10064-021-02158-w.

[21] Alwalan, M., et al., *Axial Loading Effect on the Behavior of Large Helical Pile Groups in Sandy Soil.* Arabian Journal for Science and Engineering, 2022. 47(4): p. 5017-5031. https://doi.org/10.1007/s13369-021-06422-9.

[22] Elsherbiny, Z.H., et al., *Axial compressive capacity of helical piles from field tests and numerical study.* Canadian Geotechnical Journal, 2013. 50(12): p. 1191-1203. https://cdnsciencepub.com/doi/10.1139/cgj-2012-0487.

[23] Al-Baghdadi, T., et al. *Modelling of laterally loaded screw piles with large helical plates in sand*. in *Frontiers in offshore geotechnics III: proceedings of the 3rd international symposium on frontiers in offshore geotechnics (ISFOG 2015)*. 2015. Taylor & Francis Books Ltd. https://www.proquest.com/docview/2115979801?pq-origsite=gscholar&fromopenview=true.

[24] Matlock, H., et al., *Generalized solutions for laterally loaded piles.* Journal of the Soil Mechanics and foundations Division, 1960. 86(5): p. 63-92. https://ascelibrary.org/doi/abs/10.1061/JSFEAQ.0000303.

[25] Zhang, D.J.Y., *predicting capacity of helical screw piles in alberta soils.pdf*, in *Civil and Environmental Engineer*. 1999, Alberta: Edmonton, Alberta. https://era.library.ualberta.ca/items/77edf5ee-1e61-4227-b841-b79384dd1055.

[26] Poulos, H.G., et al. *The role of analytical geomechanics in foundation engineering*. in *Foundation engineering: Current principles and practices*. 1989. ASCE. https://www.researchgate.net/publication/285678658_Role_of_analytical_geomechanics_in_foundation_engineering/citations.

[27] Terzaghi, K., *Theoretical soil mechanics*. 1943. https://libarch.nmu.org.ua/bitstream/handle/GenofondUA/19513/fe8e4061e420c7a5c38e39e9774911c0.pdf?sequence=1.

[28] Poulos, H.G., et al., *Pile foundation analysis and design*. Vol. 397. 1980: Wiley New York. https://www.academia.edu/45196632/Pile_Foundation_Analysis_and_Design_H_G_Poulos.

[29] Woodward, R.J., et al., *Drilled pier foundations.* 1972.

[30] Das, B.M., et al., *Principles of foundation engineering*. 2018: Cengage learning. https://researchonline.jcu.edu.au/42286/6/42286%20Das%20and%20Sivakugan%202017.pdf.

[31] Standard, B., *BS-8004-1986-Code of Practice for Foundations*. 10-1998, BSI.